

Validation and Optimization of Digital Breast Tomosynthesis Reconstruction using an Anthropomorphic Software Breast Phantom

Predrag R. Bakic, Susan Ng*, Peter Ringer*, Ann-Katherine Carton,
Emily F. Conant, and Andrew D.A. Maidment

University of Pennsylvania, Department of Radiology, 3400 Spruce St., Philadelphia PA 19104

*Real-Time Tomography, LLC, 1709 Balsam Lane, Villanova, PA 19085.

[Predrag.Bakic | Ann-Katherine.Carton | Emily.Conant | Andrew.Maidment] @uphs.upenn.edu

*[Susan.Ng | Peter.Ringer] @realtimetomography.com

ABSTRACT

A digital breast tomosynthesis (DBT) reconstruction algorithm has been optimized using an anthropomorphic software breast phantom. The algorithm was optimized in terms of preserving the x-ray attenuation coefficients of the simulated tissues. The appearance of the reconstructed images is controlled in the algorithm using three input parameters related to the reconstruction filter. We varied the input parameters to maximally preserve the attenuation information. The primary interest was to identify and to distinguish between adipose and non-adipose (dense) tissues. To that end, a software voxel phantom was used which included two distinct attenuation values of simulated breast tissues. The phantom allows for great flexibility in simulating breasts of various size, glandularity, and internal composition. Distinguishing between fatty and dense tissues was treated as a binary decision task quantified using ROC analysis. We defined the reconstruction geometry to enable voxel-to-voxel comparison between the original and reconstructed volumes. Separate histograms of the reconstructed pixels corresponding to simulated adipose and non-adipose tissues were computed. ROC curves were generated by varying the reconstructed intensity threshold; pixels above the threshold were classified as dense tissue. The input parameter space was searched to maximize the area under the ROC curve. The reconstructed phantom images optimized in this manner better preserve the tissue x-ray attenuation properties; concordant results are seen in clinical images. Use of the software phantom was successful and practical in this task-based optimization, providing ground truth information about the simulated tissues and providing flexibility in defining anatomical properties.

Keywords: Mammography, digital breast tomosynthesis, anthropomorphic phantom, x-ray image simulation, tomographic reconstruction, optimization of imaging systems.

1. INTRODUCTION

Digital breast tomosynthesis (DBT)¹ is undergoing final system development and initial clinical trials.^{2,3} Optimization of DBT is typically based upon the use of physical measures, or subjective comparison of clinical images. While clinical trials represent the preferred validation approach they pose a practical limitation; it is not feasible to conduct clinical trials for a large number of system configuration combinations. We have developed a preclinical optimization method based upon the analysis of simulated images of an anthropomorphic breast software phantom. The optimization method is well suited for quantitative assessment as the phantom provides ground truth about the spatial distribution of simulated tissue and tissue properties.

The goals of this research are to validate and optimize DBT reconstruction methods. Our initial effort was to reconstruct images which best portray linear x-ray attenuation coefficients of the breast tissue for the task of estimating breast density, an image-based biomarker of breast cancer risk.⁴ This work is an extension of our previous analysis of dense tissue regions extracted from clinical tomosynthesis images.⁵⁻⁷ In our previous research, we calculated the spatial correlation between regions of dense tissue segmented from the orthogonal DBT projection image and the central reconstructed image.⁶ While changing the DC component of the DBT reconstruction filter frequency response, we searched for the best spatial matching (estimated using the Jaccard coefficient⁸) between the segmented regions from projection and central reconstruction images. Such an analysis of clinical images is, however, limited by the lack of

ground truth about the extent of dense tissue regions. As an alternative, in this paper we describe the validation results based upon the use of an anthropomorphic breast phantom which provides known ground truth about the position and properties of the simulated tissues.

2. METHODS

2.1. Anthropomorphic software breast phantom

The anthropomorphic software breast phantom used in this project was developed previously, based upon a detailed analysis of breast anatomy visualized by clinical imaging and sub-gross pathology.⁹⁻¹² A phantom is created algorithmically from geometric primitives, and stored as a 3D voxel array at a user-specified spatial resolution. Each voxel belongs to a unique tissue structure, characterized by physical properties of that tissue (e.g., linear x-ray attenuation, tissue elasticity, etc.)

The software phantom allows for great flexibility in simulating breasts of various size, glandularity, and internal composition. The phantom generation starts from a realistic breast (skin) surface. The phantom interior is divided into a region of predominantly adipose tissue (AT) and a region of predominantly fibroglandular tissue (FGT). Within these large scale regions, we simulated tissue details (e.g., adipose compartments, Cooper's ligaments, and glandular tissue). Figure 1(a) shows a vertical section through the software breast phantom. The adipose compartments and Cooper's ligaments are simulated using a region-growing algorithm.¹² The region-growing algorithm includes heuristic rules governing selection of seed points and growth parameters.

2.2. DBT image acquisition and reconstruction

DBT images were reconstructed from simulated x-ray projections through the software phantom. The phantom was deformed to model mammographic compression, based upon a finite element model of 50% reduction in compressed phantom thickness.¹³ The phantom projections were simulated using a model of mono-energetic x-ray acquisition without scatter. Values of the linear x-ray attenuation coefficients were selected as 0.456 cm^{-1} for adipose tissue, 0.802 cm^{-1} for glandular and connective tissue and skin, and $0.94 \times 10^{-3} \text{ cm}^{-1}$ for air, assuming an x-ray energy of 20 keV.¹⁴ The simulated DBT acquisition geometry corresponds to a GE DBT prototype system (Senographe DS, General Electric Healthcare, Chalfont St. Giles, U.K.). We assumed a source – detector distance of 66 cm and a digital x-ray detector with $100 \mu\text{m}/\text{pixel}$ spatial resolution and a $23 \text{ cm} \times 19 \text{ cm}$ field-of-view. Fifteen DBT projections were simulated within an angular range of ± 20 degrees. An anti-scatter grid was not simulated. Figure 1(b) shows an example of a simulated DBT projection through the phantom.

A commercial back-projection filtered DBT reconstruction algorithm developed by Real Time Tomography (RTT), LLC (Villanova, PA) was used. Implemented on a GPU, the algorithm offers real-time reconstruction. It allows arbitrary selection of pixel size and slice spacing, ensuring that the reconstructed volume identically matches the phantom voxel spacing and alignment. We have used a breast phantom generated with 200 micron/voxel spatial resolution. The phantom contained a total of 56 million voxels, corresponding to a 450 ml phantom breast size.

The reconstruction software offers numerous filter implementations. A custom parameter-driven user interface provides external control of the reconstruction, allowing full exploration of the filter parameter space. In this project, we explored a parameterized Fourier-domain filter developed by RTT for the purpose of estimating breast density. We have focused on three parameters which control (i) the low frequency response shape ("LF Shape"), (ii) the mid frequency maximum ("MF Maximum"), and (iii) the mid frequency bandwidth ("MF Bandwidth"). A total of 120 filter parameter combinations were chosen for analysis.

2.3. ROC analysis

Distinguishing between the two simulated tissue types was treated as a binary decision task quantified using ROC analysis. The phantom images were reconstructed with a $200 \mu\text{m}/\text{pixel}$ spatial resolution, matching the volume resolution of the phantom. We performed voxel-to-voxel comparison between the original and reconstructed volumes. Figure 1(c) shows an example of DBT reconstructed image corresponding to the phantom section shown in Figure 1(a).

Separate histograms of the reconstructed image intensities corresponding to the true adipose and true non-adipose voxels were calculated. The adipose and non-adipose tissue regions were segmented by thresholding the histograms of

the reconstructed images. By varying the threshold values and calculating fractions of correctly and incorrectly classified voxels for each threshold value, we generated an ROC curve corresponding to each combination of filter parameters. The histograms of the reconstructed pixels corresponding to adipose and dense tissues, and the ROC curve calculated for the optimal set of reconstruction parameters, are shown in Figure 2. We selected the optimal combination of the reconstruction filter parameters as the one yielding the maximum area under the ROC curve (AUC); this parameter combination provides an image with the most accurate portrayal of the breast tissue. In addition, an experienced clinical breast radiologist reviewed reconstructed images corresponding to the maximum AUC.

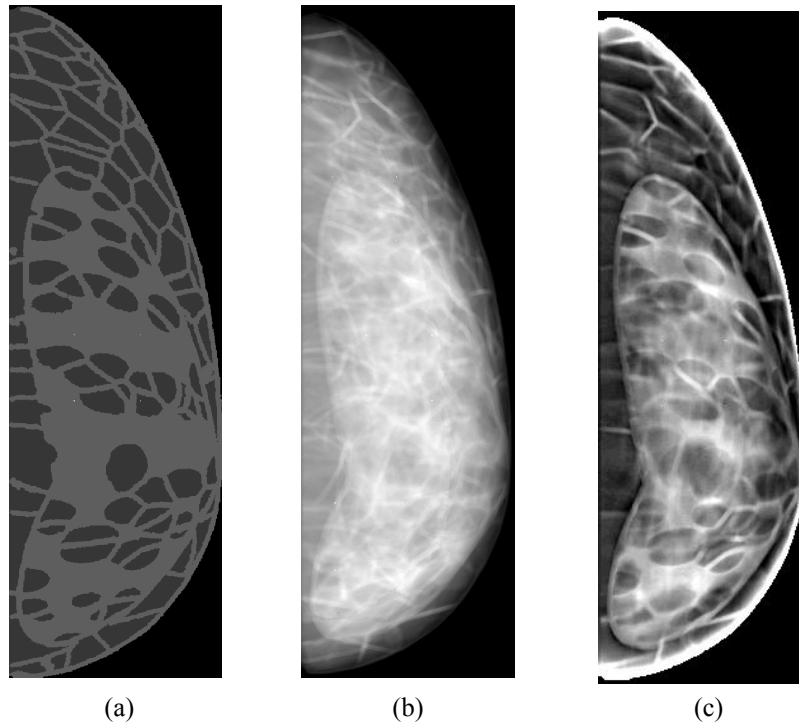


Fig. 1: (a) A section of the phantom showing simulated adipose (dark gray) and non-adipose tissues (bright gray). (b) A phantom DBT projection, simulated assuming monoenergetic x-ray beam without scatter. (c) A section of the reconstructed phantom DBT volume, corresponding to the phantom section from (a).

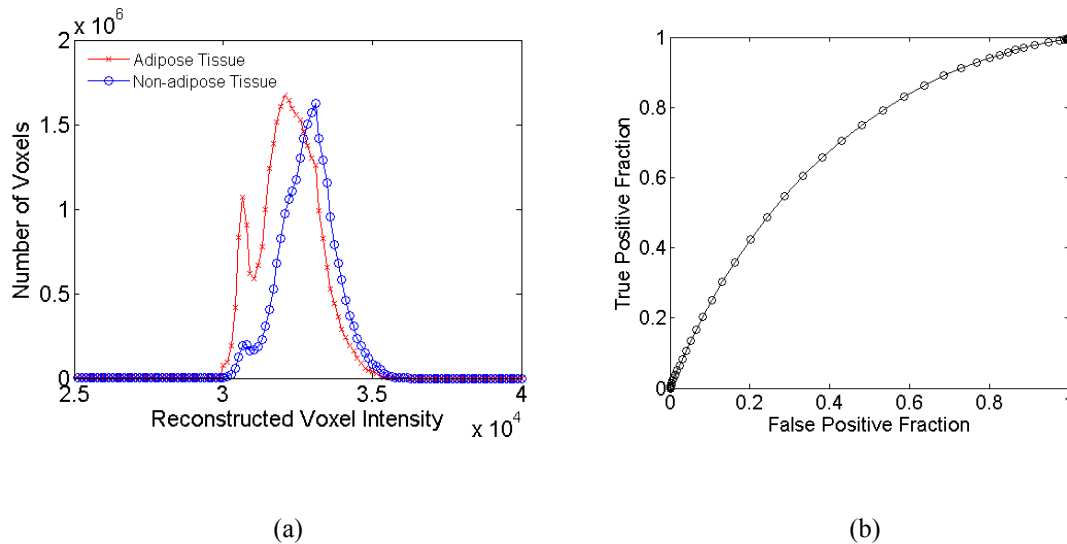


Fig. 2: (a) The histograms of reconstructed pixels corresponding to adipose and non-adipose tissues, and (b) the ROC curve generated using the histograms from (a).

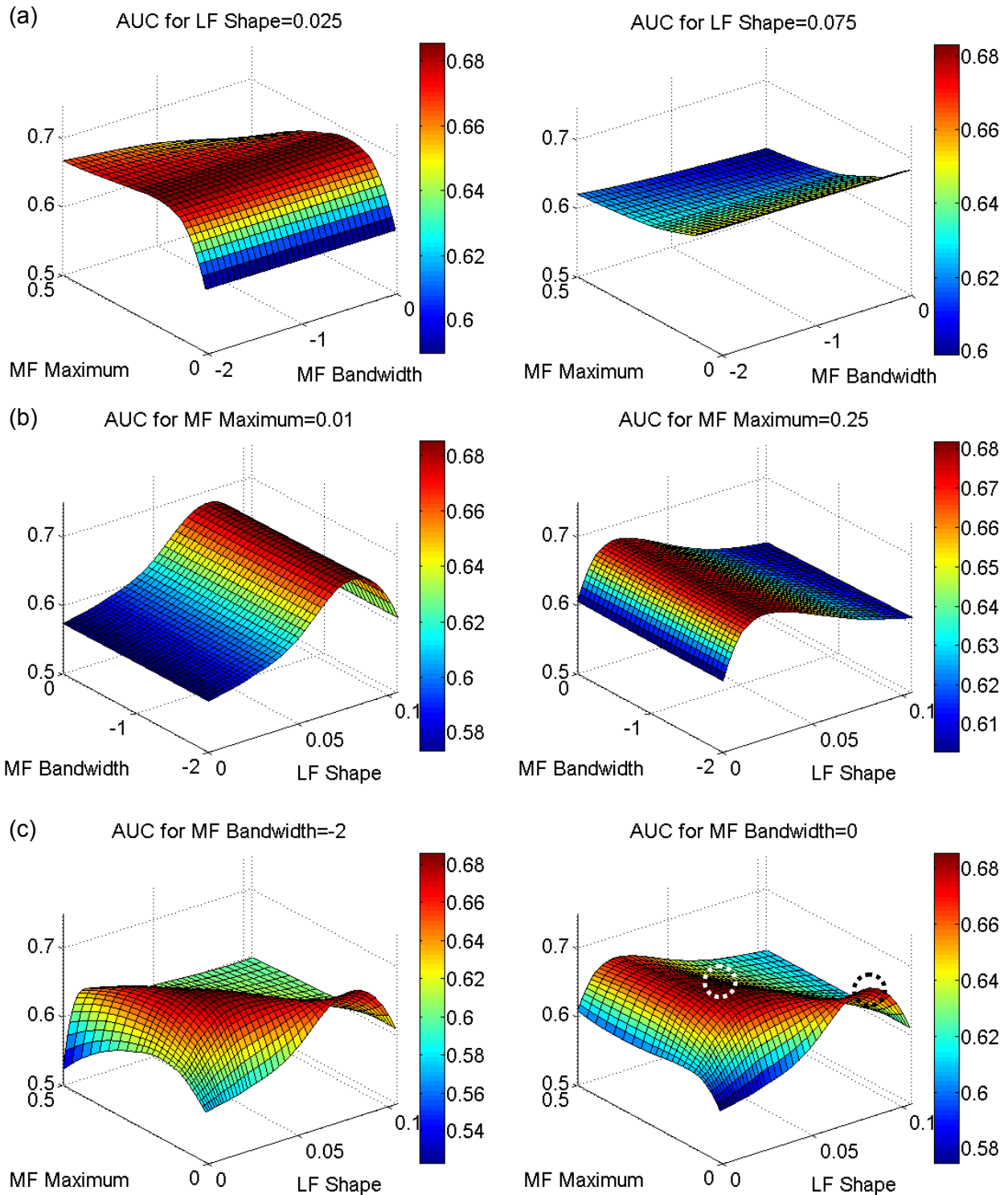


Fig. 3: Dependence of the AUC on the analyzed reconstruction filter parameters, while keeping constant (a) LF Shape parameter, (b) MF Maximum parameter, and (c) MF Bandwidth parameter. The global and local maxima of the AUC are indicated in (c) by black and white circles, respectively.

3. RESULTS

In total we explored 120 filter parameter combinations. The analysis results are summarized in Figure 3, illustrating the values of the AUC as a function of the selected filter parameters. In each figure we varied a pair of filter parameters while keeping the third parameter constant. Figure 3(a) shows AUC as a function of the MF Maximum and MF Bandwidth parameters for two different values of LF Shape parameter. Similarly, Figure 3(b) was generated while keeping MF Maximum constant and Figure 3(c) was generated while keeping MF Bandwidth constant.

One can see from Figures 3(a) and 3(b) that the AUC values have very little dependence on the MF Bandwidth parameter. Figures 3(a) also shows that for a given value of the LF Shape parameter, one can identify the optimal MF Maximum value which maximizes the AUC. Similarly, in Figure 3(b), for a given value of the MF Maximum parameter, there is an optimal LF Shape which maximizes the AUC. Figure 3(c) shows a more complex AUC dependence on reconstruction filter parameters, while keeping MF Bandwidth constant. For a given value of MF Bandwidth, one can identify a locus of points for which the AUC is near maximal. The global maximum AUC=0.683 is indicated in Figure 3(c) by a dashed black circle. The white dashed circle indicates the local maximum AUC=0.681. Note that, although corresponding to different sets of the reconstruction filter parameters, the global and local AUC maxima differ by less than 1%.

The global maximum AUC corresponds to a broad spectral coverage of the reconstructed image intensities with suppressed high frequencies; the reconstructed images are relatively uniform across the entire breast. Figure 4(a) shows the central reconstructed slice corresponding to the global maximum AUC. The reconstructed images corresponding to the local maximum AUC=0.681, were preferred by our reference radiologist due to better preservation of the edge information. Figure 4(b) shows the central reconstructed slice corresponding to the local maximum AUC.

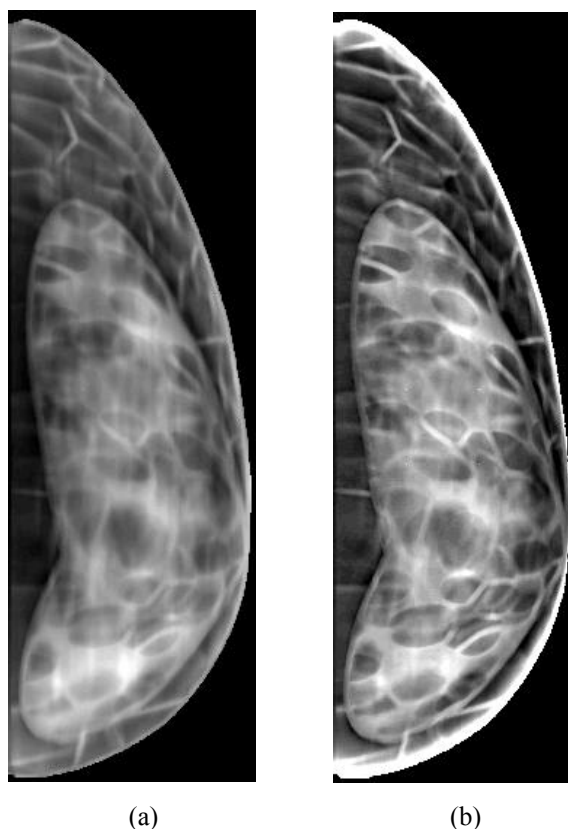


Fig. 4. Central slices of the reconstructed phantom volume corresponding to (a) the global and (b) local maximum AUC, (indicated in Figure 3(c)).

Figure 5 shows examples of clinical DBT images reconstructed using the optimal reconstruction filter parameters. These images have been reconstructed from DBT projections acquired previously in an IRB-approved, NCI/NIH-funded clinical study at the University of Pennsylvania (P01 CA85484, PI: Schnall). After providing informed consent, the women participating in that study had a DBT exam performed on a GE Senographe DS DBT prototype; this is the same system that we simulated. As discussed above, Fig. 5(b) corresponds to the reconstruction parameters setting preferred by radiologists. Fig. 5(a) provides marginally superior AUC, but results in a reconstruction that appears less sharp. However, as with the phantom images, the global maximum results in a more uniform appearance in clinical images, which leads to more accurate tissue segmentation.

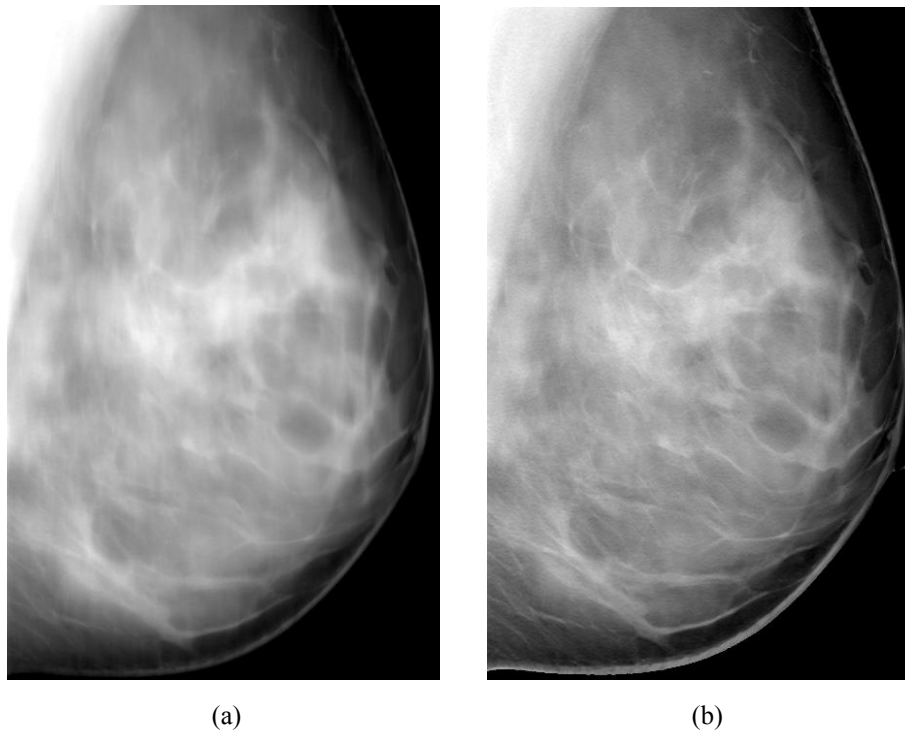


Fig. 5: Examples of clinical images of the same breast, reconstructed using the filter parameters corresponding to (a) the global and (b) local maximum AUC.

4. DISCUSSION

The presented approach allows quantitative assessment of reconstructed image quality based upon the ground truth provided by the phantom. The validation is task specific. Validation based upon various imaging tasks can be designed and performed using this approach. We described results of the validation aimed at preserving x-ray attenuation of simulated breast tissue; a similar validation procedure can be proposed for the simulated breast lesion detection task.

Our work to optimize DBT reconstruction to maximally preserve the breast tissue attenuation properties was motivated by a desire to estimate breast density in DBT. The standard method for estimating breast density (Cumulus, v. 4.0, University of Toronto) is based upon interactive thresholding of mammographic images.¹⁵ This 2D approach is limited by the projective nature of mammographic images. Methods for estimating the 3D (volumetric) breast density have been developed and reported in the literature.¹⁶⁻¹⁸ Those methods are predicated upon certain assumptions about the breast shape and compressed breast thickness to estimate the proportion of adipose and dense tissue. These assumptions pose certain limitations to the accuracy of the estimation of volumetric breast density. DBT, as a 3D breast imaging modality offers an alternative approach to estimating volumetric breast density. Our preliminary assessment of breast density estimation from DBT images has revealed its limitations due to the use of limited number of x-ray projection angles in DBT acquisition.^{5,6} The limited angle acquisition results in the contribution of out-of-plane densities to the

DBT reconstructed images. DBT images, optimally reconstructed as described in this work, provide the best preservation of the tissue x-ray attenuation information, thus minimizing the out-of-plane contribution. Such reconstructed images could be used for breast density estimation by either thresholding image intensities, or by the quantitative analysis of the reconstructed image intensities.

We identified several limitations of the presented study. The simulated DBT image acquisition assumed monoenergetic x-ray beam without scatter and without quantum noise. The acquisition simulation can potentially be modified to include more detailed models of x-ray spectra and detector models. An alternative approach is to apply the described ROC analysis approach to images of our physical phantom (Figure 5), fabricated based upon the software breast phantom.¹⁹ We also used only one phantom in this study, although our software phantom provides flexibility to cover a wide range of anatomic variations. Error bars of the AUC values can be calculated by analyzing phantoms of the same size and glandularity with different composition. We can also analyze the effects of breast size, compressed thickness, and glandularity by analyzing appropriately designed software phantoms.



Fig. 5: Photograph of a physical anthropomorphic breast phantom designed based upon our software breast phantom.

Further extension of the described validation approach can be based upon the inclusion of a simulated observer, either in the form of a general model of human visual properties (as, e.g., JNDmetrix²⁰), or a detailed simulation of breast lesions and background tissues and the use of e.g., channelized Hotelling observer model²¹. We can also implement a more efficient search for the global AUC maximum. In this paper we used a “brute-force” search by testing individually a large number of predetermined filter parameter combinations from a regularly organized 3D grid. Alternatively, we could use methods such as simulated annealing²² which may improve the efficiency and accuracy of the optimization. We can also simulate other modalities, e.g., breast ultrasound, dynamic contrast-enhanced magnetic resonance imaging, or contrast enhanced mammography or DBT.

5. CONCLUSION

We have developed a method for optimizing DBT reconstruction algorithms for specific imaging tasks using simulated images of an anthropomorphic software breast phantom. In this paper, we have demonstrated the use of this method for the task of preserving breast tissue x-ray attenuation coefficients. This task was chosen as being relevant in estimating breast density, a known biomarker of breast cancer risk. Optimal images were obtained using reconstructions produced with filter parameters that provide broad spectral coverage in the Fourier domain, resulting in reconstructed images with

relatively uniform intensities across the area of the breast. The described approach has value in preclinical optimization of breast density estimation algorithms. Adaptation of this method to other clinical tasks may aid in the design of DBT clinical trials by identifying the most promising imaging devices and performing initial system configuration optimization *in silico*.

6. ACKNOWLEDGEMENT

This work in progress has been supported by a subcontract from NIH R44 EB07140 (Real Time Tomography, LLC.) Previous research on software phantoms was funded by NSF Grant IRI-9504363 (PI: Brzakovic), NIH Grant P01 CA85484 (PI: Schnall), a subcontract from NIH R01 CA102758 (PI: Glick University of Massachusetts; subcontract PIs: Bakic and Maidment), and Susan G. Komen Breast Cancer Foundation Research Grant BCTR133506 (PI: Bakic). The contents of this paper are solely the responsibility of the authors and do not necessarily represent the official views of the various funding agencies.

REFERENCES

1. Niklason LT, Christian BT, Niklason LE, et al. Digital tomosynthesis in breast imaging. *Radiology*. Nov 1997;205(2):399-406.
2. Poplack S, Kogel C, Nagy H. Initial experience with digital breast tomosynthesis in 99 breasts of 98 women with abnormal digital screening mammography. Paper presented at: RSNA 2005; Chicago, IL.
3. Kopans D. Digital Breast Tomosynthesis: Experience with Imaging over 3500 Subjects Paper presented at: RSNA, 2009; Chicago, IL.
4. Martin LJ, Boyd NF. Mammographic density. Potential mechanisms of breast cancer risk associated with mammographic density: hypotheses based on epidemiological evidence. *Breast Cancer Research*. 2008;10:201-214.
5. Bakic PR, Kontos D, Carton A-K, Maidment ADA. Breast Percent Density Estimation from 3D Reconstructed Digital Breast Tomosynthesis Images. Paper presented at: Medical imaging: Physics of medical imaging; 2008, 2008; San Diego, CA.
6. Bakic PR, Kontos D, Troxel AB, Maidment ADA. Comparison of Breast Percent Density Estimated from Digital Mammograms and Central Reconstructed Tomosynthesis Slice Images. Paper presented at: 9th International Workshop on Digital Mammography, 2008; Tucson, AZ.
7. Bakic PR, Carton A-K, Kontos D, Zhang C, Troxel AB, Maidment ADA. Breast percent density estimation from mammograms and central tomosynthesis projections. *Radiology*. 2009.
8. Aiello EJ, Tworoger SS, Yasui Y, et al. Associations among circulating sex hormones, insulin-like growth factor, lipids, and mammographic density in postmenopausal women. *Cancer Epidemiol Biomarkers Prev*. 2005;14(6):1411-1417.
9. Bakic PR, Brzakovic D. Simulation of digital mammogram acquisition. In: Boone JM, Dobbins JT, eds. *SPIE Medical Imaging*. Vol 3659. San Diego, CA: SPIE, Bellingham, WA; 1999:866-877.
10. Bakic PR, Albert M, Brzakovic D, Maidment ADA. Mammogram synthesis using a 3D simulation. I. Breast tissue model and image acquisition simulation. *Medical Physics*. 2002;29(9):2131-2139.
11. Bakic PR, Albert M, Brzakovic D, Maidment ADA. Mammogram synthesis using a 3D simulation. II. Evaluation of synthetic mammogram texture. *Medical Physics*. 2002;29(9):2140-2151.
12. Zhang C, Bakic PR, Maidment ADA. Development of an Anthropomorphic Breast Software Phantom Based on Region Growing Algorithm. Paper presented at: SPIE Medical Imaging, 2008; San Diego, CA.
13. Ruiter NV, Zhang C, Bakic PR, Carton A-K, Kuo J, Maidment ADA. Simulation of tomosynthesis images based on an anthropomorphic software breast tissue phantom. In: Sonka M, Manduca A, eds. *SPIE Medical Imaging*. San Diego, CA: SPIE; 2008.
14. Johns PC, Yaffe MJ. X-ray characterisation of normal and neoplastic breast tissues. *Physics in Medicine & Biology*. 1987;32(6):675-695.
15. Byng JW, Boyd NF, Fishell E, Jong RA, Yaffe MJ. The quantitative analysis of mammographic densities. *Physics in Medicine & Biology*. 1994;39(10):1629-1638.

16. Pawluczyk O, Augustine BJ, Yaffe MJ, et al. A volumetric method for estimation of breast density on digitized screen-film mammograms. *Medical Physics*. 2003;30(3):352-364.
17. Highnam R, Pan X, Warren R, Jeffreys M, Davey Smith G, Brady M. Breast composition measurements using retrospective standard mammogram form (SMF). *Physics in Medicine and Biology*. 2006;51(11):2695-2713.
18. Highnam R, Jeffreys M, McCormack V, Warren R, Davey-Smith G, Brady M. Comparing measurements of breast density. *Physics in Medicine and Biology*. 2007;52(19):5881-5895.
19. Carton A-K, Derand H, Ullberg C, Bakic PR, Maidment ADA. Development of a 3D physical anthropomorphic breast phantom. Paper presented at: Tomosynthesis Imaging Symposium 2009: Frontiers in Research and Clinical Applications, 2009; Durham, NC.
20. Johnson J, Lubin J, Nafziger J, Krupinski E, Roehrig H. Channelized model observer using a visual discrimination model. Paper presented at: Medical Imaging 2005, 2005; San Diego, CA.
21. Gallas BD, Barrett HH. Validating the use of channels to estimate the ideal linear observer. *Journal of the Optimatl Society of America A*. 2003;20:1725-1738.
22. Laarhoven PJM, Aarts EHL. *Simulated Annealing: Theory and Applications*. Dordrecht, The Netherlands: Kluwer; 1987.